Chinese Society of Aeronautics and Astronautics
& Beihang University

Chinese Journal of Aeronautics

cja@buaa.edu.cn
www.sciencedirect.com

Transitional wave configurations between Type III and Type IV oblique-shock/bow-shock interactions

Jun PENG [a,b], **Shuai LI** [a,c], **Fan YANG** [a,c], **Mingyue LIN** [a,c,*], **Guilai HAN** [a,c], **Zongmin HU** [a,c]

[a] *State Key Laboratory of High-temperature Gas Dynamics, Institute of Mechanics, Chinese Academy of Sciences, Beijing 100190, China*
[b] *The System Design Institute of Mechanical-Electrical Engineering, Beijing 100854, China*
[c] *School of Engineering Science, University of Chinese Academy of Sciences, Beijing 100049, China*

Abstract The interactions of oblique/bow shock waves are the key flow phenomena restricting the design and aerothermodynamic performance of high-speed vehicles. Type III and Type IV Shock/Shock Interactions(SSIs) have been extensively investigated, as such interactions can induce abnormal aerodynamic heating problems in hypersonic flows of vehicles. The transition process between these two distinct types of shock/shock interactions remains unclear. In the present study, a subclass of shock/shock interaction configuration is revealed and defined as Type IIIa. Type IIIa interaction can induce much more severe aerodynamic heating than a Type IV interaction which was ever reported to be the most serious in literature. The intense aerodynamic heating observed in this configuration highlights a new design point for the thermal protection system of hypersonic vehicles. A secondary Mach interaction between shock waves in the supersonic flow path of a Type III configuration is demonstrated to be the primary mechanism for such a subclass of shock/shock interaction configuration.
© 2022 Chinese Society of Aeronautics and Astronautics. Production and hosting by Elsevier Ltd. This is an open access article under the CC BY-NC-ND license (http://creativecommons.org/licenses/by-nc-nd/4.0/).

1. Introduction

The interactions of oblique/bow shock waves, as key flow phenomena around hypersonic vehicles, have been investigated in the past few decades. The overall interaction configuration changes diversely according to the strengths and the geometric parameters of the intersecting shock waves. As a consequence, the aerodynamic loads over the vehicle surface in the vicinity of the interaction region may vary significantly when the interaction pattern changes.[1] Edney[2–4] conducted tunnel tests as well as theoretical analyses, and defined six types of oblique/

* Corresponding author.
  E-mail address: linmingyue@imech.ac.cn (M. LIN).
Peer review under responsibility of Editorial Committee of CJA.

Production and hosting by Elsevier

bow Shock-Shock Interaction (SSI), i.e., Type I to Type VI. His research revealed abnormally high aerothermal loads induced by the Type IV SSI.[2,5,6] The aforementioned studies confirmed that the most severe pressure load and heat transfer rate occur at the point where the jet impinges at the surface of the blunt-body in a Type IV shock-shock interaction. Based on the experimental data for such an interaction configuration, the enhancement factor of the peak heat transfer rate had been approximately correlated with the peak pressure amplification, jet width, and the blunt radius.[2–5] Further experimental investigations conducted by Grasso et al.[7,8] indicated that peak heat flux arises when the jet strikes the model surface perpendicularly.

Both experimental studies[5–9] and numerical simulations[10–16] revealed that Type IV interactions feature intrinsic unsteadiness. The transition between Type IV and Type IVa interaction patterns was visualized in a run of tunnel tests.[7] The underlying mechanism was not clear and was supposed to be either the hysteresis phenomenon associated with the transition between regular and Mach reflections of shock waves[17] or the transient phenomenon occurring with the development of the test flow. Detailed numerical simulations conducted by Windisch et al.[13–16] indicated that the unsteadiness in wall pressure or heat flux is mainly correlated with the jet unsteady mechanism. Non-monotonic dependence of peak heat flux on the oblique-bow shock intersecting point was revealed in the tests.[8,18] When Type IV interaction turns into Type III accompanied by the disappearance of expansion fan in the jet structure, a second heat flux maximum is formed. Unsteady phenomena in the overall Type V SSI configuration were revealed by computational investigations on hypersonic double-wedge flows.[19–21] Here, the transition between regular reflection and Mach reflection of shock waves and the shock wave-shear layer interaction are the key issues to give rise to the unsteadiness aforementioned. When the transition between different SSI patterns occurs, high-temperature effects may lead to remarkable variation in the transition conditions.[22–28]

Since the starting studies of Edney[2–4] on the oblique/bow shock-shock interactions which lead to the definition of six types of SSI, extensive investigations either by experiment or computation have been reported in the literature. However, to the best of the authors' knowledge, the transition criteria among different SSI types have not been obtained to date due to the complexity of the flow field. A preliminary study using a machine learning method from Peng et al presented the SSI transition criteria for Type III-IV, and Type IV-IVa, respectively.[29] However, Type IV and Type IVa interactions are hard to distinguish due to the inherent unsteady features. In addition, there are significant differences in the overall wave configurations of Type III and Type IV interactions as shown in Fig. 1[2]. In Fig. 1, IS repesents incident shock wave, BS repesents bow shock wave, TS repesents transmitted shock wave, SL repesents shear layer, NS repesents normal shock wave. It is clear that Type III and Type IV configurations cannot turn from one into the other like an on-off switch and there should be a transition process between them. The non-monotonic phenomenon revealed in the heat flux measurements conducted by Boldyrev et al.[8] implies that the SSI configuration within the transition path should be significantly different from either Type III or Type IV interactions.

In this paper, the transitional flow structures between Type III and Type IV oblique shock/bow shock interactions are studied by numerical simulation. The main objective of the present work is to reveal the distinctive flow features during the transition process as well as the resulting surface quantities such as pressure and heat flux.

2. Computation setting

2.1. Model definition

The present work focuses on shock/shock interactions during the transition process between Type III and Type IV SSI configurations. According to the parameter-correlation study conducted by Peng et al.,[29] the control parameters for such a shock-dynamics dominant problem includes three variables, i.e., the freestream Mach number, Ma_∞, the incident shock angle, β, and the geometrical parameter I_r which determines the spatial relation between the incident shock wave (IS) and the bow shock wave (BS). All the control parameters are schematically depicted in Fig. 2. Two of the above-mentioned parameters, i.e., Ma_∞ and β can uniquely determine the flow solutions in regions (2), (3) and (4) based on the classically two- and three-shock theories proposed by von Neumann.[30] Φ represents the angle of circumferential position on the circular surface, and R is the radius of the cylinder. Parts of the remaining flow regions can be theoretically obtained when I_r is given simultaneously. However, there
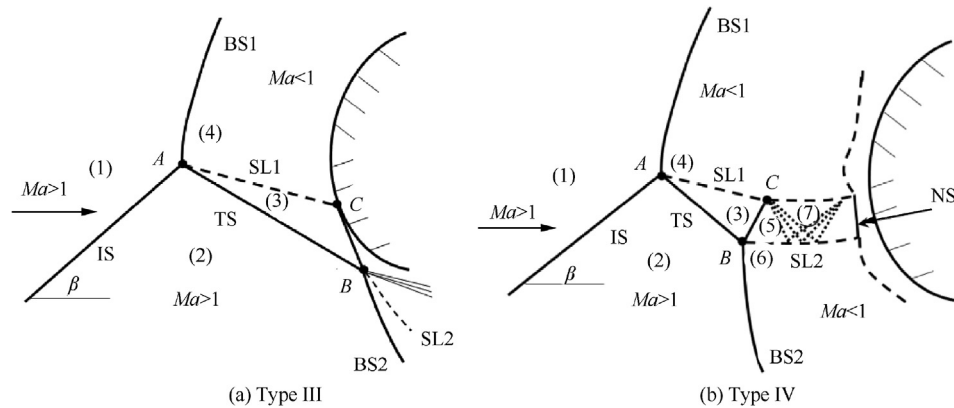

Fig. 1 Type III and Type IV shock/shock interaction configurations according to Edney's definition.[2]
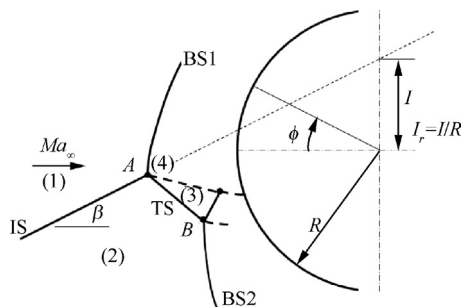
Fig. 2 Control parameters for flows of Type III and Type IV shock-shock interactions.
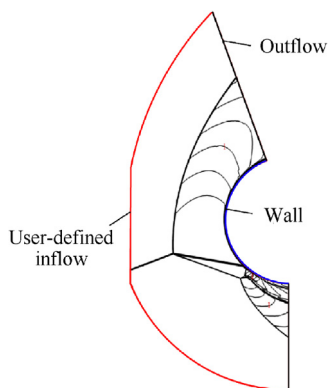

Fig. 3 Computational domain, boundary specifications and overall SSI configuration shown by Mach number contour (Grid: 1600×800, $Ma_\infty = 8$, $\beta = 21°$, $I_r = 0.17$).

are no theoretical solutions to the coordinates of triple points A and B by far to the best of the authors' knowledge. Thus, such SSI problems cannot be solved theoretically, but can be worked out by numerical simulation.[10–16,29]

Two-dimensional laminar compressible Navier-Stokes equations are supposed to be the governing equations for the flows studied hereafter. For the numerical algorithms, the second-order TVD (Total Variation Diminishing) scheme based on a non-linear Riemann solver named HLLC (Harten-Lax-van Leer Contact)[31] is applied to solve the convective terms. This computational code based on the finite-volume method has been validated in the previous investigations[29] for the simulations of hypersonic flows especially Type IV oblique shock/bow shock interactions. It is verified that the distributions of heat flux calculated by the code used in this paper are in good agreement with the experimental data, including the locations and magnitudes of peaks of heat flux.

2.2. Convergence study

The computational domain used in the following simulations is given in Fig. 3. The domain is discretized by structured grid while the grid is refined both in the shock-shock interaction region and along the cylinder surface. The SSI configuration for the following conditions ($Ma_\infty = 8$, $\beta = 21°$, $I_r = 0.17$) is depicted in the figure by the contour of flow Mach number. For all the following computations, the domain should be adjusted carefully to maintain that the sonic lines downstream the bow shock waves should be completely accommodated inside. Boundary specifications are also shown in Fig. 3. The boundary conditions are set to user-defined inflow and outflow at the left and right of the computational domain respectively.
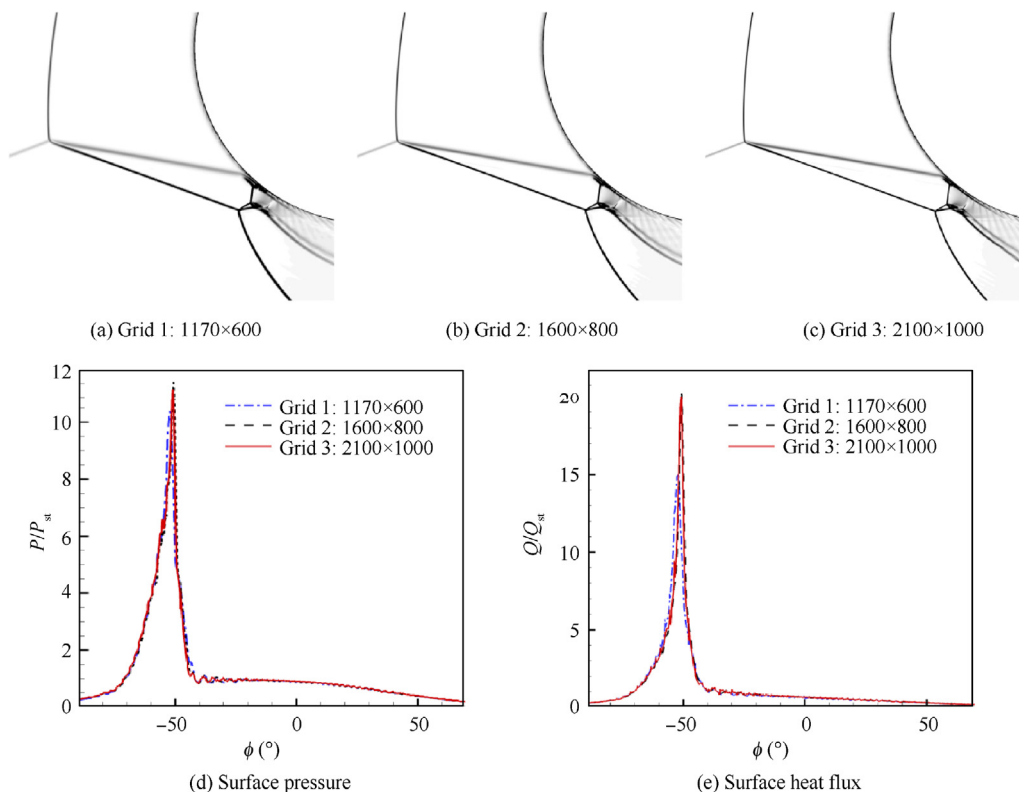

(a) Grid 1: 1170×600

(b) Grid 2: 1600×800

(c) Grid 3: 2100×1000

(d) Surface pressure

(e) Surface heat flux

Fig. 4 Grid independence evaluation for simulations of oblique shock/bow shock interactions ($Ma_\infty = 8$, $\beta = 21°$, $I_r = 0.17$).

Nonslip and isothermal conditions are used for the solid wall at a fixed temperature of 300 K. For all the computations in the present study, the static temperature and pressure of the freestream airflow are given as $T_\infty = 200$ K, $P_\infty = 428$ Pa, respectively. The freestream flow conditions are selected according to the test flow conditions of a large-scale detonation-driven shock tunnel located at the State Key Laboratory of High-temperature Gas Dynamics of Institute of Mechanics of Chinese Academy of Sciences in Beijing.[32–34] The unit Reynolds number of the flow is 1.27×10^6/m. When the model is small and the boundary layer is not fully developed, the flow is generally laminar. Thermal equilibrium gas is utilized in this study, thermodynamic and transport properties of which are calculated by polynomials of temperature.[35] The polynomials reflect the vibration excitation of air molecules at high temperatures. Of all the cases studied in this paper, the maximum temperature of the flow field is about 2800 K. The degree of the dissociation of molecular is small, if any. Therefore, turbulence and other dissipative phenomena are not considered.

It should be pointed out that the main purpose of the present work is to illustrate the shock-dynamic features during the transition process between Type III and Type IV shock-shock interactions. Grid independence evaluation, here, primarily aims at the shock-dynamics dominant issues of SSI and the

surface quantities like pressure or heat flux. Three sets of the grid are used in the comparative computations ($Ma_\infty = 8$, $\beta = 21°$, $I_r = 0.17$), and the outputs are given in Fig. 4. The scale of the first grid along the cylinder surface is maintained to be 1×10^{-6} m which corresponds to $y^+ \approx 1$. The overall SSI flow structure is depicted by density gradient

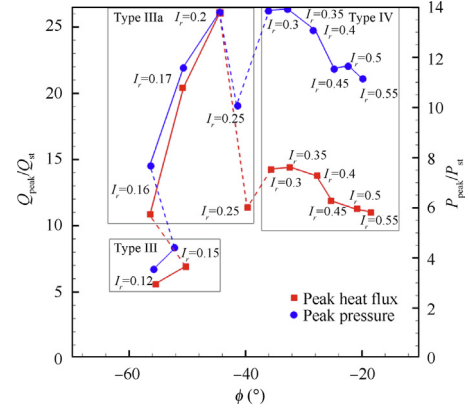**Fig. 6** Peak heat flux and peak pressure during the transition of Type III-IV shock/shock interaction ($Ma_\infty = 8$, $\beta = 21°$).
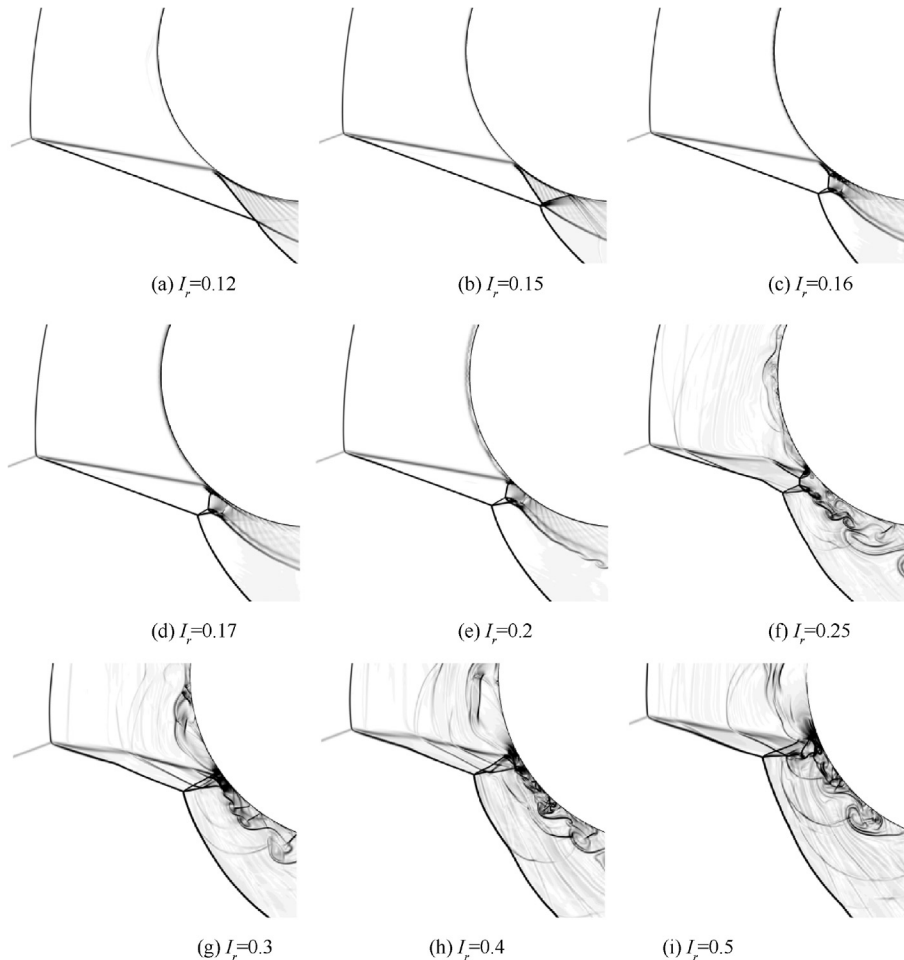

(a) I_r=0.12

(b) I_r=0.15

(c) I_r=0.16

(d) I_r=0.17

(e) I_r=0.2

(f) I_r=0.25

(g) I_r=0.3

(h) I_r=0.4

(i) I_r=0.5

Fig. 5 SSI transition from Type III to Type IV with rising geometrical parameter I_r ($Ma_\infty = 8$, $\beta = 21°$).

(a) Schematic diagram   (b) Zoom-in view   (c) Numerical result

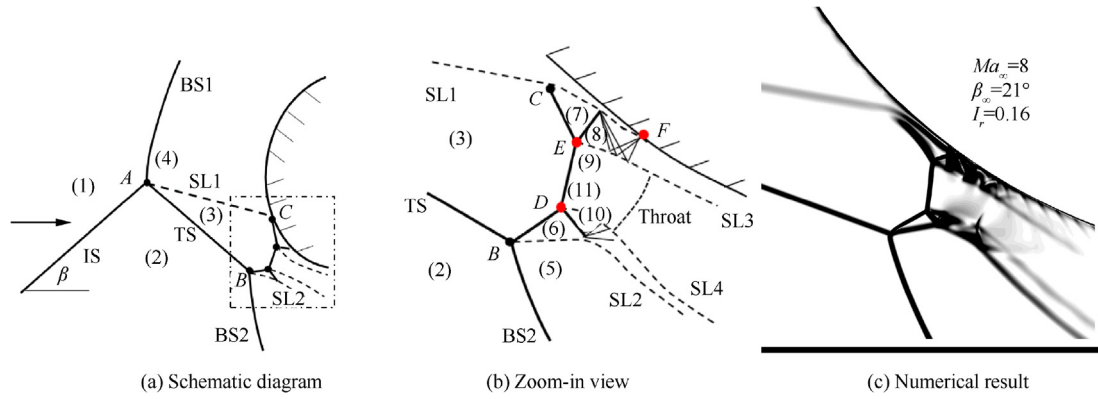**Fig. 7** Sketch and zoom-in flow structure of Type IIIa shock/shock interaction (corresponding to Fig. 5(c) where $Ma_\infty = 8$, $\beta = 21°$, $I_r = 0.16$).

$|\nabla \rho| = \sqrt{\left(\frac{\partial \rho}{\partial x}\right)^2 + \left(\frac{\partial \rho}{\partial y}\right)^2}$ and respectively shown in Fig. 4 (a)-Fig. 4(c) for each computation, while the comparison of surface quantities is given in Fig. 4(d) or Fig. 4(e). The results of grid independence study clearly show that all the three grids are sufficient to capture the key flow phenomena (see Fig. 4 (a)-Fig. 4(c)), like Mach stem and contact surface, and the surface quantities obtained by Grid 2 (1600 × 800) and Grid 3 (2100 × 1000) are nearly identical. The comparison indicates that the density of Grid 2(1600 × 800) is sufficiently high for capturing the shock-dynamics dominant phenomena of interest in the present work and will be used in the following simulations.

3. Results

3.1. Type IIIa shock/shock interaction

Different SSI types can be obtained by changing I_r while maintaining Ma and β constant. As aforementioned, the flow states in each region around triple point A (see Fig. 1 or Fig.2) can be determined once Ma and β are given. The flow states include the thermodynamic and kinematic parameters in regions (2), (3) and (4). However, triple point A must move as I_r changes to feel the disturbance which is generated by impingement of the shear layer, SL1, over the cylinder surface and propagates

upstream in the subsonic flow of region (4). Consequently, the SSI configuration can vary from Type I to Type VI with the increase of I_r. Fig. 5 shows the wave structures of different SSI types when I_r increases from 0.12 to 0.5 while maintaining $Ma_\infty = 8$, and $\beta = 21°$.
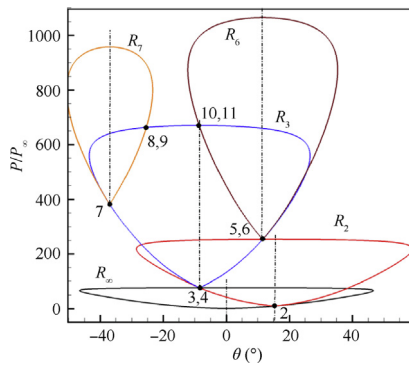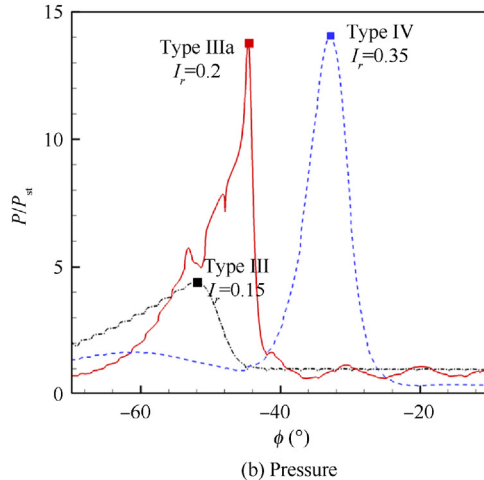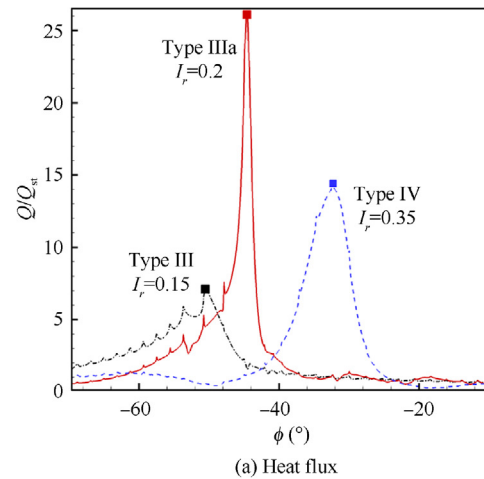

(a) Heat flux

(b) Pressure

Fig. 9 Typical profiles of heat flux and pressure) along the cylinder surface for Type IIIa ($I_r = 0.2$) and Type IV ($I_r = 0.35$) interactions ($Ma_\infty = 8$, $\beta = 21°$).

Fig. 8 Shock polar system for Type IIIa interaction (corresponding to Fig. 5(c)) ($Ma_\infty = 8$, $\beta = 21°$, $I_r = 0.16$).

According to the sketch in Fig. 1, it is easy to find a typical Type III configuration of SSI as depicted in Fig. 5(a) for the simulation when $I_r = 0.12$. Fig. 5(b) follows the main features of Type III interaction configuration while a little different from Fig. 5(a) appears in the vicinity of point B (see labels in Fig. 1) which becomes a triple point of a Mach reflection. In Fig. 5(a), B is a point of intersection of two oblique shock waves of the same family. On the other hand, Type IV interactions for $I_r = 0.3, 0.4$ and 0.5 are given in Fig. 5(g), Fig. 5(h) and Fig. 5(i), respectively. As Type IV SSI is reported to be unsteady mainly due to jet impingement,[13–16] the present simulations for the aforementioned three conditions appear unsteady too. Each frame here shows a transient SSI structure for each condition of I_r.

The SSI structures depicted in the remaining frames, i.e., Fig. 5(c)-Fig. 5(e), are different from either Type III or Type IV in the vicinity of point B (see labels in Fig. 1) when the supersonic flow in region (3) arrives at the cylinder surface. This kind of SSI structure occurs within a relatively small parameter domain of $I_r = 0.16 - 0.2$ for the given conditions $\beta = 21°$ and $Ma_\infty = 8$. Here, this special situation is classified as Type IIIa shock/shock interaction to make difference from Edney's terminology of Type III. Obviously, the overall structure of Type IIIa interaction looks similar to that of a general Type III interaction while appears subtle differences in the vicinity of interaction region near the cylinder surface from the latter. Therefore, Type IIIa configuration is a subclass of Type III interaction patterns. It was reported in the literature[2–8] that Type IV interference results in the most critical dynamic and thermal loads associated with perpendicular jet impingement on the surface. From the present study as depicted in Fig. 6, the studied SSI structure of Type IIIa can lead to more severe aerodynamic heating than Type IV. In Fig. 6, the peak heat flux and pressure are nondimensionalized by the heat flux, Q_{st} (3.5×10^5 W/(m^2·s)) and pressure, P_{st} (3.58×10^4 Pa), at the stagnation point of the cylinder surface without shock interference, respectively.

The distinctive feature of Type IIIa SSI is schematically depicted in Fig. 7 with a zoom-in illustration (see Fig. 7(b)) for the local wave pattern in the vicinity of triple point B. The theoretical solution of this special kind of wave system can be obtained by shock polar analysis as shown in Fig. 8
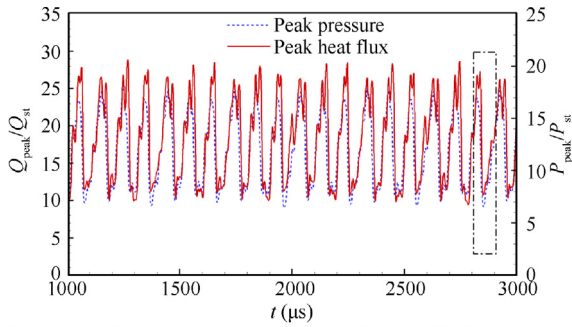

Fig. 10 Peak heat flux and pressure for Type IIIa interaction with oscillation ($I_r = 0.25$, $Ma_\infty = 8$, $\beta = 21°$).

Fig. 12 Sketch of double-InMR structure of unsteady Type IIIa SSI at $t = 2800$ μs ($I_r = 0.25$, $Ma_\infty = 8$, $\beta = 21°$).

(a) $t=2800$ μs   (b) $t=2810$ μs   (c) $t=2820$ μs   (d) $t=2830$ μs   (e) $t=2840$ μs

(f) $t=2850$ μs   (g) $t=2860$ μs   (h) $t=2870$ μs   (i) $t=2880$ μs   (j) $t=2890$ μs

Fig. 11 Transient flow structures of Type IIIa interaction with oscillation ($I_r = 0.25$, $Ma_\infty = 8$, $\beta = 21°$).

Fig. 13 Peak heat flux and its location along the cylinder surface (labels a to j correspond to each frame in Fig. 11).

Fig. 14 Peak heat flux and pressure for Type IV interaction with oscillation ($I_r = 0.4$, $Ma_\infty = 8$, $\beta = 21°$).

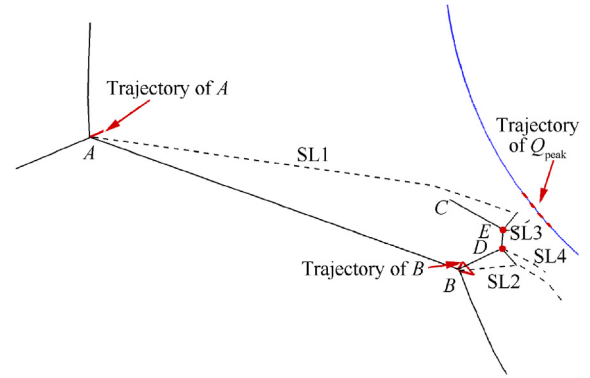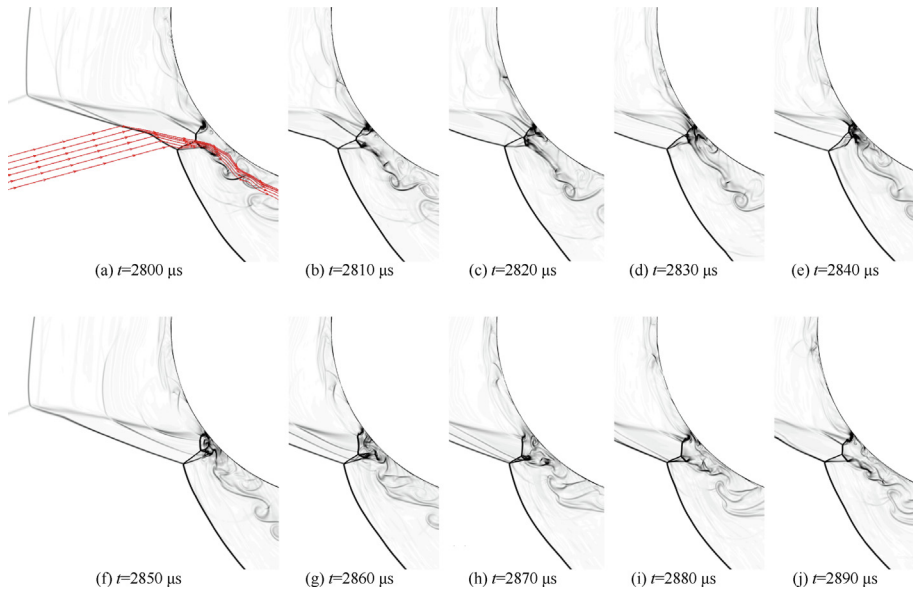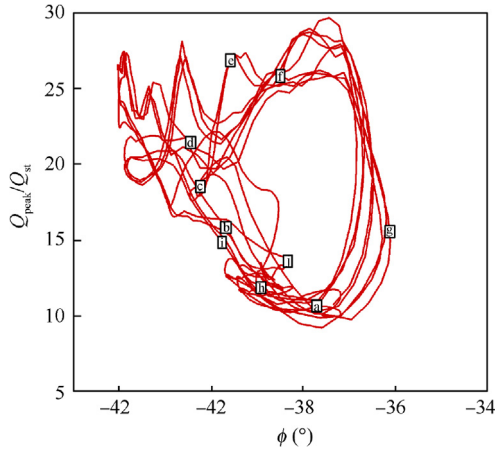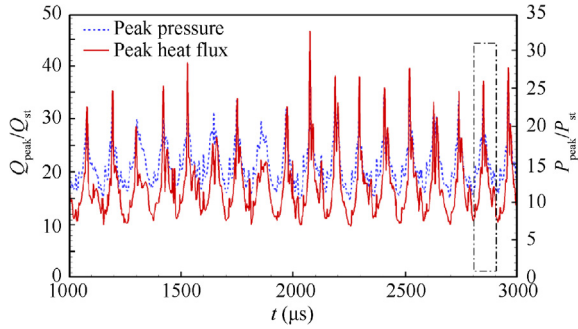for the case of $I_r = 0.16$. When the supersonic flow between the shear layer SL1 and the transmitted shock TS, both of which originate from triple-point A approaches the cylinder

surface, an oblique shock wave, i.e., CE (see Fig. 7(a)) is formed to match the boundary conditions along the surface. The interaction of the oblique shock CE and the reflected shock BD originating from triple-point B results in a bi-Mach reflection structure and forms new triple-points, D and E. Two shear layers, SL3 and SL4, come into being and form a convergent-divergent flow tube. Such a bi-Mach reflection structure is defined as double-DiMR by Li et al.[36] and can maintain steady in steady supersonic flows. As a consequence, the flow structures of Type IIIa interaction as depicted in Fig. 5(c)-Fig. 5(e) are always steady unlike Type IV interaction which is substantially unsteady.

Shear layers SL1 and SL3 assemble a supersonic jet developing along the cylinder surface. The reflected shock wave of the triple-wave structure at point E is reflected repeatedly between the two shear layers. As schematically depicted in Fig. 8, the flow in region (7) is close to the sonic flow condition; a Mach disc appears at point F (see Fig. 7(b)) in the supersonic jet. The interaction between the aforementioned Mach disc with the shear layer SL1 leads to an extremely high heating load shortly downstream point F. As the parameter I_r increases with the translational moving of the incident shock, the aforementioned triple-wave structure will shrink and the supersonic jet flow surrounded by SL1 and SL3 will get thinner. When $I_r = 0.2$, the peak heat flux becomes around twenty-six times the corresponding value at the stagnation point, as can be seen in Fig. 6, i.e., $Q_{peak(Ir=0.2)} / Q_{st} \approx 26$. Such an amplification factor of aerodynamic heating is much higher than the maximum amplification factor induced by the Type IV interaction when $I_r = 0.35$. The distribution profiles of heat flux and pressure along the cylinder surface for Type III, Type IIIa and Type IV interactions are combined in Fig. 9 for a direct comparison.

3.2. Type IIIa shock/shock interaction with oscillations

The Type IIIa SSI structures as depicted in Fig. 5 (c)-Fig. 5(e) are steady with the aid of a convergent-divergent flow tube

(a) t=2815 μs   (b) t=2825 μs   (c) t=2835 μs   (d) t=2845 μs   (e) t=2855 μs

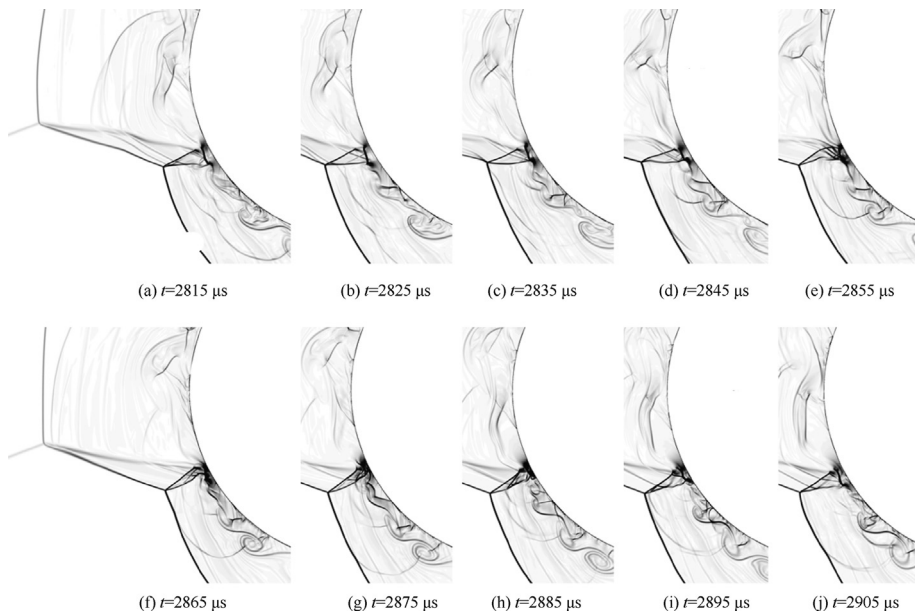(f) t=2865 μs   (g) t=2875 μs   (h) t=2885 μs   (i) t=2895 μs   (j) t=2905 μs

Fig. 15 Transient flow structures of Type IV interaction with oscillation ($I_r = 0.4$, $Ma_\infty = 8$, $\beta = 21°$).

downstream the Mach stem DE (see Fig. 7(b)). With the increase of the geometric factor I_r, the tripe-wave structure at point E will shrink and disappear completely at a critical condition, e.g., $I_r = 0.2$ for $Ma_\infty = 8$, $\beta = 21°$. At such a critical point, the shock wave DE intersects with the shear layer SL1 perpendicularly and triggers unsteadiness. As a consequence, the overall structure of such a special Type IIIa interaction undergoes approximately periodic oscillation which can be reflected by the history of the peak heat flux or the peak pressure along the cylinder surface as given in Fig. 10. The frequency of the oscillation is around 11 kHz. The transient flow structures within one cycle (corresponding to the time range enclosed by the dash-dotted box in Fig. 10) are depicted in Fig. 11.

The unsteadiness of Type IIIa structure as shown in Figs. 10 and 11 are primarily induced by the interaction of the shock wave DE and the shear layer SL1. Fig. 12 schematically shows the transient wave configuration corresponding to the transient structure of Type IIIa interaction at $t = 2800$ μs depicted by the first frame of Fig. 11. The aforementioned shock-shear layer interaction results in a λ-shaped structure or a Mach reflection structure at triple-point E. The two shear layers, i.e., SL3 and SL4, assemble a divergent flow tube locally, indicating that the transient double-Mach reflection structure connected by DE is unsteady in nature. Such a shock structure is denoted as double-InMR by Li et al.[36] which is not physical in steady flows. Shocklets or perturbation waves propagate upstream during the unsteady evolution of the double-Mach reflection structure and influence the triple-points A and B. However, the influences are so gentle that the trajectories of points A and B during an oscillation period are confined in tiny domains as demonstrated in Fig. 12 by the line segment and triangle, respectively.

The peak heat flux and the corresponding location (represented by parameter φ) at each time transient associated with each frame in Fig. 11 are depicted in Fig, 13. The peak varies from around ten to twenty-nine times of the stagnation heat flux, while its location varies within 6 degrees of φ. The peak heat flux reaches a maximum at time transient of 2840 μs shortly after the birth of a new double-I nMR structure. It should be noted that the peak heat flux given in Fig. 6 for the case of $I_r = 0.25$ is the temporal average as it varies with time. Oscillations of the wave structure leads to a decrease in the averaged heat flux at each point of the cylinder surface.

The fact that a Type IV interaction is substantially unsteady is widely reported in the literature.[5–16] Unlike a Type III or IIIa interaction in which the shear layer SL2 does not reach the cylinder, both primary shear layers of a Type IV interaction, i.e., SL1 and SL2 (see the definition in Fig. 1(b)), strike the cylinder surface and induce a supersonic jet impingement. Such an impingement can result in severe heating and pressure loads to the surface accompanied by flow oscillations as depicted in Fig. 14 for the case of $I_r = 0.4$ for instance. The frequency of the oscillation is around 10 kHz for this case, within which the main flow structures are shown in Fig. 15. As the supersonic jet flow in region (3) is approximately perpendicular to the cylinder surface, a normal shock wave, as denoted by NS in Fig. 1(b), appears and interacts with the shear layers. The normal shock wave varies in length and location slightly and becomes the shortest and nearest to the surface at a time transient of about 2865 μs (see Fig. 15) when the peak heat flux reaches maximum.

As discussed hereinbefore, the unsteady behavior of Type IIIa interaction is different from that of Type IV interaction. The primary difference is associated with the local wave structures at the spot where the supersonic jet impinges the cylinder surface. The historic variation of peak heat flux and surface pressure as respectively shown in Figs. 10 and 14 reflect the aforementioned difference.
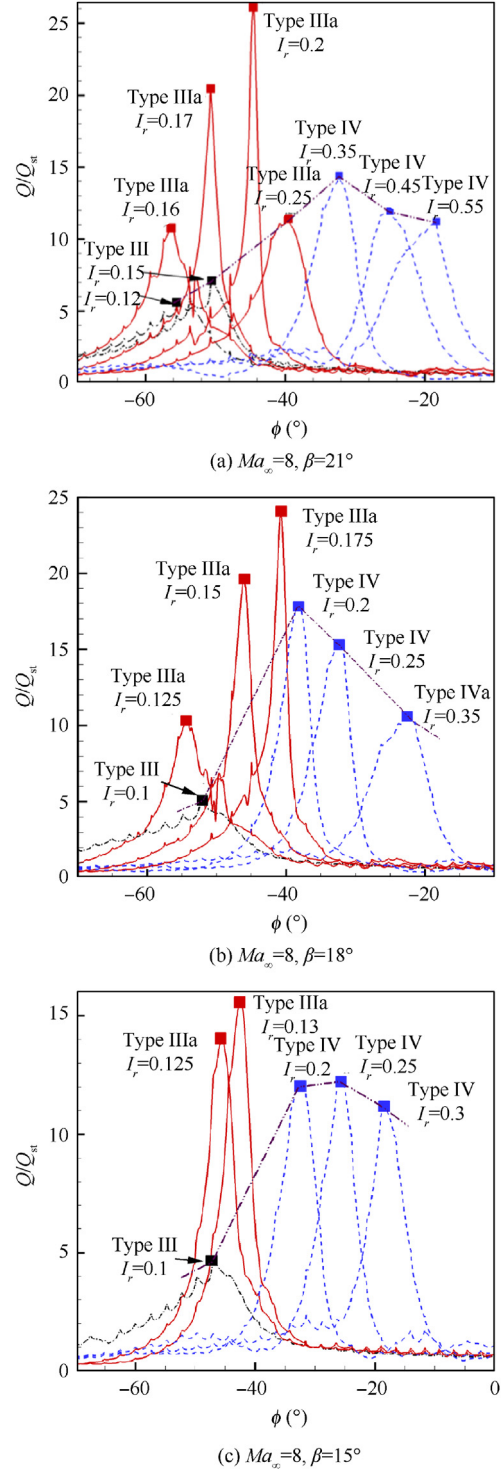

Fig. 16 Profiles of surface heat flux for different types of shock-shock interaction configuration.

3.3. Discussion

The Type IIIa SSI studied here is a subclass wave configuration of Type III interaction that generally results in the most severe aerodynamic heating in the interference region along the cylinder surface. Such a wave configuration occurs during the transition domain between Type III and IV SSI, and combines the primary flow features of the latter two interaction patterns. The peak heat flux induced by the Type IIIa SSI within a special range of parameter I_r may become much larger than that in a Type IV SSI with the same Ma_∞ and β as can be seen in Fig. 16. The most serious aerodynamic heating conditions may be misestimated if one applies interpolation among predicted solutions of Type III and IV interaction. However, a Type IIIa SSI occurs within a very small parameter domain of I_r as shown in Fig. 16. Therefore, the flow structures of Type IIIa interaction can hardly be visualized by hypersonic tunnel tests and have not been paid careful attention to in open literature, according to the best of the authors' knowledge.

As can be seen in Figs. 7 and 8, the Mach type interaction between oblique shock waves *CE* and *BD* gives birth to a Type IIIa SSI configuration. Here, shock *CE* is induced by the interaction of the supersonic flow in region (3) while *BD* is the reflected shock wave of the Mach reflection wave configuration associated with Triple-point *B*. When shear layers SL3 and SL4 assemble a convergent-divergent flow tube as depicted in Fig. 7, the resulting Type IIIa SSI configuration maintains steady, and is not vice versa as illustrated by Figs. 10 to 13. Nevertheless, a regular interaction instead of a Mach interaction between shock waves *CE* and *BD*, is theoretically accepted as shown in Fig. 17 where a smaller incident shock angle is given, i.e., $\beta = 15°$. Solution states (8,9) in the shock polar diagram represent the regular interaction aforementioned. Such a Type IIIa SSI configuration always maintains steady since the flow is always supersonic downstream the regular interaction. Fig. 16 (c) indicates that the peak heat flux in a Type IIIa SSI with regular shock/shock interaction in the supersonic flow path between shear layers can exceed that of a Type IV configuration.

Borovoy et al. revealed a non-monotonic distribution of the peak heat flux with the peak position by experimental measurements using specially arranged thermal couples.[8,18] The first maximum peak heat flux is associated with the supersonic jet impingement in a Type IV shock/shock interaction. A great number of studies have been concentrated on such kind of interaction and thrown light on the aerodynamic mechanisms. Borovoy et al. stated that the second maximum is primarily due to the disappearance of an expansion fan in the supersonic jet when Type IV flow turns into Type III flow. According to the present study, the primary mechanism of the second maxima of peak heat flux is related to subclass of Type III shock/shock interaction, i.e., Type IIIa, occurring during the transition between Type III and Type IV. In addition, the main inducement of a Type IIIa configuration is the Mach interaction or regular interaction between two shock waves of different families in the supersonic flow path between shear layers as depicted in Fig. 5(d)-Fig. 5(f) or Fig. 17(b), respectively. However, due to the insufficient resolution of flow visualization in experiments or of numerical simulation.[8,18] around twenty years back, such a subtle flow structure could not be well captured.

4. Conclusions

In the present study, the flow patterns during the transition between Type III and Type IV oblique shock/bow shock interactions over a cylinder model are numerically simulated. A geometric ratio I_r is introduced to represent the spatial relation between the incident shock wave and the cylinder surface. I_r is one of the control parameters of the studied problems along with the incident shock angle, β, and the freestream flow Mach number, Ma_∞. By carefully adjusting parameter I_r while maintaining the rest control parameters fixed, different types of shock/shock interaction configurations are obtained in the simulations. SSI configuration can vary from Type I to Type VI when I_r changes, which has been widely reported. However, a transition SSI configuration between Type III and Type IV which has not been paid careful attention to is found in this work, when I_r is located inside a very small range of parameter domain.

This subclass of Type III shock/shock interaction configuration is revealed and defined as Type IIIa SSI. Such an interaction configuration occurs during the transition process between Type III and Type IV SSI configurations and appears different flow features in a subtle region from both of the latter. A Mach interaction or regular interaction between
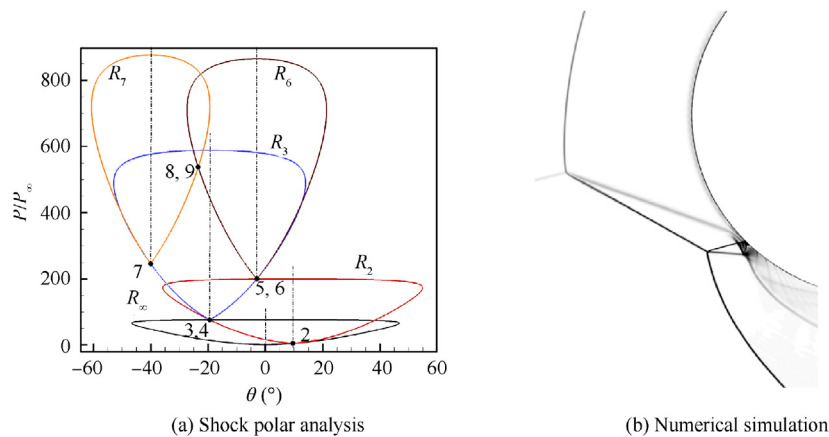

(a) Shock polar analysis   (b) Numerical simulation

Fig. 17 Type IIIa SSI configuration with regular shock-shock interaction in supersonic jet flow ($I_r = 0.125$, $Ma_\infty = 8$, $\beta = 15°$).

two shock waves of different families in the supersonic flow path between shear layers of the primary triple-points is found to be the main mechanism for the birth of a Type IIIa SSI configuration. Such a local shock/shock interaction can be either steady or unsteady depending on whether a convergent-divergent flow tube is formed or not downstream the local interaction. The aforementioned local shock/shock interaction results in a secondary shock wave/shear layer interaction along the cylinder surface which may induce an extremely high heat flux. The most severe aerodynamic heating condition occurs when a Type IIIa configuration is steady. In fact, the transient peak of heat flux in the unstable Type IIIa interaction (such as the case given in Fig. 11) can be higher than a Type IV interaction. However, the location of the peak heat flux varies along the cylinder surface which may significantly decrease the time-averaged peak of heat flux.

This is a primary study using numerical techniques for high-temperature gas flows without considering turbulence in the simulations. In the future, turbulent simulation or experimental visualization will be conducted for further studies on such special type of shock/shock interaction.

Declaration of Competing Interest

The authors declare that they have no known competing financial interests or personal relationships that could have appeared to influence the work reported in this paper.

Acknowledgements

References

1. Xiang GX, Wang C, Teng HH, et al. Shock/shock interactions between bodies and wings. *Chin J Aeronaut* 2018;**31**(2):255–61.
2. Edney BE. Anomalous heat transfer and pressure amplification on blunt bodies at hypersonic speeds in the presence of an impinging shock. Stockholm: Flygtekniska Forsoksanstalten Aeronautical Research Institute of Sweden; 1968. Report No.: FFA-115.
3. Edney BE. The effects of shock impingement on the heat transfer around blunt bodies at M = 4.6 and 7. *2nd aerodynamic testing conference*. Reston: AIAA;1966.
4. Edney BE. Effects of shock impingement on the heat transfer around blunt bodies. *AIAA J* 1968;**6**(1):15–21.
5. Holden M, Moselle J, Wieting A, et al. Studies of aerothermal loads generated in regions of shock, shock interaction in hypersonic flow. *26th aerospace sciences meeting*; 1988 Jan 11 - 14; Reno. NV. Reston: AIAA; 1988.
6. Wieting AR, Holden MS. Experimental shock-wave interference heating on a cylinder at Mach 6 and 8. *AIAA J* 1989;**27** (11):1557–65.
7. Grasso F, Purpura C, Chanetz B, et al. Type III and type IV shock/shock interferences: Theoretical and experimental aspects. *Aerosp Sci Technol* 2003;**7**(2):93–106.
8. Boldyrev SM, Borovoy VY, Chinilov AY, et al. A thorough experimental investigation of shock/shock interferences in high Mach number flows. *Aerosp Sci Technol* 2001;**5**(3):167–78.
9. Khatta A, Gopalan J. Hypersonic shock tunnel studies of Edney Type III and IV shock interactions. *Aerosp Sci Technol* 2018;**72**:335–52.
10. Lind C, Lewis M. A numerical study of the unsteady processes associated with the typeIV shock interaction. *29th joint propulsion conference and exhibit*; 1993 Jun 28-30; Monterey, CA. Reston: AIAA; 1993.
11. Lind CA, Lewis MJ. Computational analysis of the unsteady type IV shock interaction of blunt body flows. *J Propuls Power* 1996;**12** (1):127–33.
12. Gaitonde D, Shang JS. On the structure of an unsteady type IV interaction at Mach 8. *Comput Fluids* 1995;**24**(4):469–85.
13. Zhong XL. Application of essentially nonoscillatory schemes to unsteady hypersonic shock-shock interference heating problems. *AIAA J* 1994;**32**(8):1606–16.
14. Furumoto G, Zhong XL, Furumoto G, et al. Numerical simulation of viscous unsteady type IV shock-shock interaction with thermochemical nonequilibrium. *35th aerospace sciences meeting and exhibit*; 1997 Jan 6–9; Reno. NV. Reston: AIAA; 1997.
15. D'Ambrosio D. Numerical prediction of laminar shock/shock interactions in hypersonic flow. *J Spacecr Rockets* 2003;**40** (2):153–61.
16. Windisch C, Reinartz BU, Müller S. Investigation of unsteady edney type IV and VII shock-shock interactions. *AIAA J* 2016;**54** (6):1846–61.
17. Wang D, Yu Y. Shock wave configurations and reflection hysteresis outside a planar Laval nozzle. *Chin J Aeronaut* 2015;**28**(5):1362–71.
18. Borovoy VY, Chinilov AY, Gusev VN, et al. Interference between a cylindrical bow shock and a plane oblique shock. *AIAA J* 1997;**35**(11):1721–8.
19. Ben-Dor G, Vasilev EI, Elperin T, et al. Self-induced oscillations in the shock wave flow pattern formed in a stationary supersonic flow over a double wedge. *Phys Fluids* 2003;**15**(12):L85–8.
20. Hu ZM, Gao YL, Myong RS, et al. Geometric criterion for RR↔MR transition in hypersonic double-wedge flows. *Phys Fluids* 2010;**22**(1):016101.
21. Hu ZM, Myong RS, Wang C, et al. Numerical study of the oscillations induced by shock/shock interaction in hypersonic double-wedge flows. *Shock Waves* 2008;**18**(1):41–51.
22. Sanderson SR, Hornung HG, Sturtevant B. Aspects of planar, oblique and interacting shock waves in an ideal dissociating gas. *Phys Fluids* 2003;**15**(6):1638–49.
23. Sanderson SR, Hornung HG, Sturtevant B. The influence of non-equilibrium dissociation on the flow produced by shock impingement on a blunt body. *J Fluid Mech* 2004;**516**:1–37.
24. Xiong W, Li J, Zhu Y, et al. RR-MR transition of a Type V shock interaction in inviscid double-wedge flow with high-temperature gas effects. *Shock Waves* 2018;**28**(4):751–63.
25. Li J, Zhu YJ, Luo XS. On Type VI-V transition in hypersonic double-wedge flows with thermo-chemical non-equilibrium effects. *Phys Fluids* 2014;**26**(8):086104.
26. Nompelis I, Candler GV, Holden MS. Effect of vibrational nonequilibrium on hypersonic double-cone experiments. *AIAA J* 2003;**41**(11):2162–9.
27. Peng J, Zhang ZJ, Hu ZM, et al. A theoretical and computational study of the vibration excitation on the transition criteria of shock wave reflections. *Aerosp Sci Technol* 2019;**89**:299–306.
28. Zhang ZJ, Wen C, Zhang WS, et al. A theoretical method for solving shock relations coupled with chemical equilibrium and its applications. *Chin J Aeronaut* 2022;**35**(6):47–62.
29. Peng J, Luo CT, Han ZJ, et al. Parameter-correlation study on shock-shock interaction using a machine learning method. *Aerosp Sci Technol* 2020;**107**:106247.
30. von Neumann J. Refraction, intersection and reflection of shock waves. Washington, D.C.: NAVORD; 1943. Report No.: 203-45.
31. Batten P, Leschziner MA, Goldberg UC. Average-state jacobians and implicit methods for compressible viscous and turbulent flows. *J Comput Phys* 1997;**137**(1):38–78.
32. Jiang ZL. Experiments development of long-test-duration hyper-velocity detonation-driven shock tunnel (LHDst). *52nd aerospace*

sciences meeting; 2014 Jan 13 - 17; National Harbor, Maryland. Reston: AIAA; 2014.

33. Jiang ZL, Yu HR. Theories and technologies for duplicating hypersonic flight conditions for ground testing. *Natl Sci Rev* 2017;**4**(3):290–6.

34. Liu MK, Han GL, Jiang ZL. Experimental study on the evolution of mode waves in laminar boundary layer on a large-scale flat plate. *Phys Fluids* 2022;**34**(1):013612.

35. McBride B, Zehe M, Gordon S. NASA Glenn coefficients for calculating thermodynamic properties of individual species. Washington, D.C.: NASA; 2002. Report No.: NASA/TP-2002-211556.

36. Li H, Chpoun A, Ben-Dor G. Analytical and experimental investigations of the reflection of asymmetric shock waves in steady flows. *J Fluid Mech* 1999;**390**:25–43.